# A Search for the $K_s^0$ in $\tau^-$ Decays at LEP

Aaron Giles

April 21, 1992

## 1 Introduction

This paper presents an analysis of the $\tau^- \to K_s^0 X^- \nu_\tau$ decay mode,[1] including a measurement of the inclusive branching ratio for this process. With the aid of the OPAL detector and reconstruction programs, candidate events were selected from a pool of 37 964 $\tau^-$ decays produced at LEP in 1990 and 1991. The $K_s^0$ was then identified via its decay into a $\pi^+\pi^-$ pair within the detector volume by reconstructing the decay vertex and determining the invariant mass of the system. A companion Monte Carlo sample was used in the identification of background sources and for calculating the detection efficiencies needed to compute the final branching ratio value.

The decay modes of the $\tau^-$ lepton present a rich source for exploring the coupling of the $W^\pm$ boson to hadronic final states. Unlike its lighter brothers, the $e^-$ (which cannot decay at all) and the $\mu^-$ (which can only decay weakly into $e^-\bar{\nu}_e\nu_\mu$), the $\tau^-$ can decay into any of a number of hadronic as well as leptonic final states via the exchange of a virtual $W^\pm$. In particular, a more precise knowledge of the decay mode $\tau^- \to K_s^0 X^- \nu_\tau$ is useful in studying the $s$ quark and its coupling to the $W^\pm$, as shown in Figure 1 in the case of a $K_s^0\pi^-$ final state.

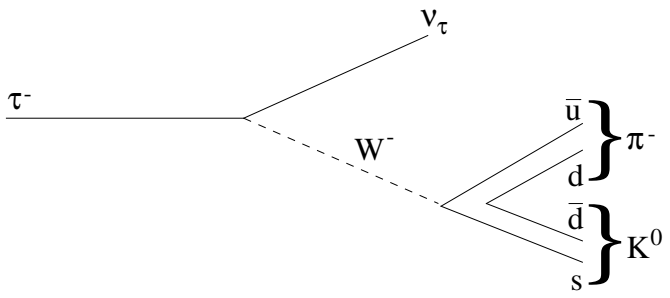


Figure 1: *An example of a* $W^\pm$ *coupling to* $q\bar{q}$*, in this case resulting in the expected* $K_s^0$ *decay products.*

[1]Here, as well as throughout this paper, reference to $\tau^-$ properties and results apply equally well under charge conjugation to a $\tau^+$. The same is true for the $e^-$ and $\mu^-$.

Previous experiments [1] suggest that the sole source of production of the $K^0_s$ in $\tau^-$ decays is via the resonance decay of a $K^{*-}(892)$:

$$\tau^- \to K^{*-}(892)\nu_\tau \to K^0_s \pi^- \nu_\tau,$$

which would implicate the $\pi^-$ as the only decay partner of the $K^0_s$. If this hypothesis is found to be true, then the measurement of the $\tau^- \to K^0_s X^- \nu_\tau$ branching ratio that is described here will provide a direct basis for estimating the underlying $\tau^- \to K^{*-}(890)\nu_\tau$ branching ratio, both as an independent measurement and as a check on the consistency of the data sample. Thus, an examination of the source of the $K^0_s$ mesons produced is included as an important part of this analysis.

# 2 The OPAL Detector

The $\tau^-$ data used to make this measurement was collected over a two-year period (1990–1991) using the OPAL detector, which is located on the main accelerator ring at the Large Electron-Positron (LEP) collider in Geneva, Switzerland. During these two years, LEP was devoted almost entirely to producing $Z^0$ bosons by colliding the $e^+e^-$ beams together at a center of mass energy of roughly 91 GeV. The resulting $Z^0$ was then observed to decay, occasionally (on the order of 4% of the time) producing clean $\tau^+\tau^-$ events, a small subset of which are the subject of this analysis.

The OPAL (Omni-Purpose Apparatus for LEP) detector itself is a general-purpose detector designed to track the products of any event produced in the high-energy $e^+e^-$ collisions at LEP. Although the detector as a whole is a rather complicated apparatus, consisting of some 15 separate components, only three of its numerous subdetectors hold direct significance for the detection of the secondary $K^0_s$ vertex. Overall, OPAL is cylindrical in shape and is designed to be symmetric about the axis of the incoming beams. The relevant subdetectors are laid out in a similar manner, layered as cylindrical shells about the main beam pipe. This design lends itself naturally to a simple geometry where the $z$-axis is defined to point along the direction of the incoming $e^-$ beam, perpendicular to a plane defined by standard $r$-$\phi$ polar coordinates. Occasionally, the polar angle $\theta$ is used to describe particle trajectories; it is defined as in standard spherical coordinates with respect to the $z$-axis

The three detectors important to this analysis are collectively known as the central detector. These are, in order from innermost to outermost, the vertex detector, the jet chamber, and the Z-chambers. They are contained in a pressure vessel which maintains a pressure of 4 bar throughout the volume. The entire vessel is then placed inside a large solenoid which provides a constant magnetic field of 0.435 T along the $z$-axis. The specifics concerning the design and limitations of these subdetectors are outlined in the sections below. More detailed information can be found in [2].

## 2.1 The Vertex Detector

The vertex detector is a small, high resolution drift chamber designed to measure the positions of outgoing charged particles immediately upon their leaving the beam pipe.

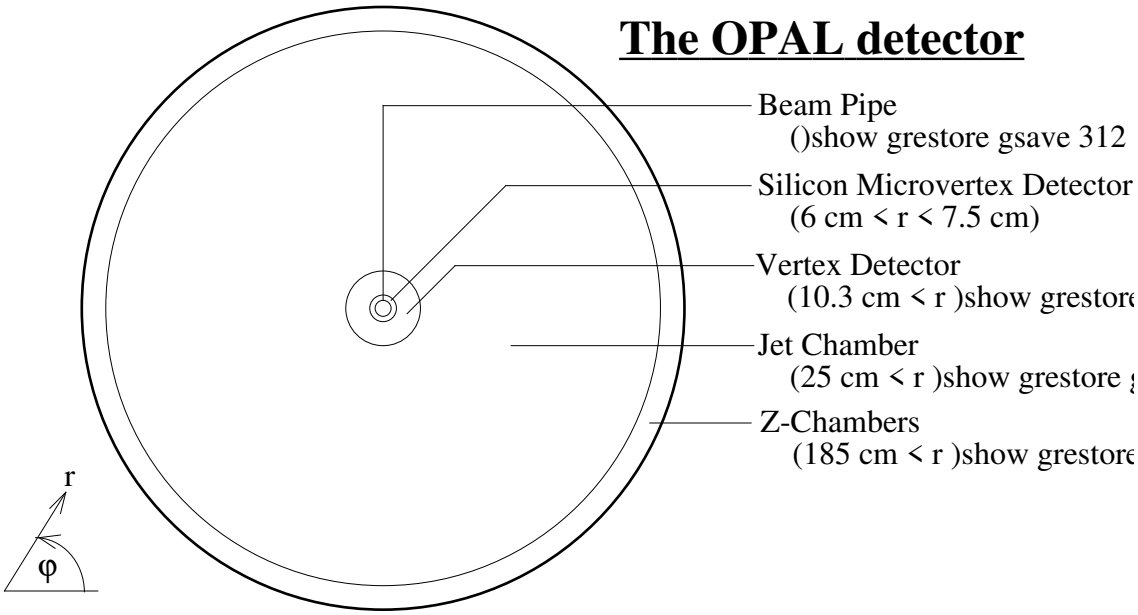


Figure 2: *A cross section of the OPAL detector. The z axis is directed perpendicular to the page.*

The chamber itself covers 100 cm along the beam axis, and measures particle positions at radii between 9 cm and 24 cm to an accuracy of 50 $\mu$m in the $r$-$\phi$ plane. Physically, the detector is composed of 36 "wedges," each covering 10° of the cylinder, and within every one of these wedges are 18 sense wires, serving as anodes to pick up any ionized electrons resulting from the passage of a charged particle.

The sense wires in the vertex detector are strung in two different ways. Innermost are the standard axial wires, 12 to a sector, which are strung strictly parallel to the beam direction. These are responsible for the detection of charged tracks between 10.3 and 16.2 cm. Outside of this area are a second set of wires, the stereo sense wires, which are strung in pairs at a modest angle of $\pm 4°$ to either side of the beam axis, forming a very flattened "X" shape. This design allows for a more precise measurement of the $z$ coordinate, because the angled sense wires are effectively measuring the track's position in a plane containing a (small) $z$ component. The domain of the stereo wires extends out to a radius of 21.3 cm.

The axial wires of the vertex detector also possess the ability to measure the $z$-coordinate of outgoing particles to a rather crude degree (4 cm). This is initially accomplished by simply comparing the time difference between signals received at each end of the sense wires. Further $z$ resolution (to 700 $\mu$m) can be achieved offline by exploiting the measurements from the stereo wires in conjunction with $r$-$\phi$ positions determined from the axial wires.

### 2.2 The Jet Chamber

The jet chamber is the primary tracking chamber for the detector, covering radii from 25 cm to 185 cm for a distance of 4 m along the beam axis. It is divided into 24 sectors of 15°, each of which contains 159 axial sense wires strung parallel to the beam direction. This setup allows measurement of track positions in the volume of the detector to an accuracy of 135 $\mu$m for each of 159 points in the $r$-$\phi$ plane.

To measure the $z$-coordinate of the outgoing tracks, the process of charge division is used. If the resistance along the sense wire is assumed to be constant, it is expected that more charge will be detected on the side with less net resistance between the ionization location and the wire's end. Thus, by comparing the charge flowing out on either end of the sense wire, an estimate of the $z$-coordinate (to within 6 cm) can be determined.

### 2.3 The Z-Chambers

Located just outside the jet chamber are the Z-chambers, a collection of 24 drift chambers designed to measure to a high precision the $z$-coordinate of particles leaving the jet chamber. Each of the Z-chambers stretches the complete 4 m along the beam axis and 50 cm in the $\phi$ direction, with a thickness of 5.9 cm. These chambers are then further subdivided into 8 cells 50 cm square, each with 6 sense wires strung azimuthally to enable tracking in the $z$ direction. Together, the collection of Z-chambers covers 94% of the azimuthal angle and is able to track the $z$-coordinate of outgoing particles to an accuracy of 300 $\mu$m.

## 3 Data Analysis

### 3.1 The Data Samples

The event samples for the two-year period being examined represent a total of over 500 000 visible $Z^0$ decays, out of which roughly 20 000 $\tau^+\tau^-$ events are expected to occur. Ideally, these events would be treated as a single large sample, produced under nearly identical circumstances. However, between the 1990 and 1991 runs of the LEP collider, a silicon microvertex detector was installed in OPAL between the beam pipe and the previously-described vertex detector. This additional material increases the chances for an unwanted interaction with an outgoing particle, thus altering the composition of the background events. To account for this discrepancy, the data from these two periods was split into two samples, with separate background and efficiency determinations made for each. After independently correcting both samples for these effects, the resulting data was then recombined to make the final branching ratio measurement.

The complete data set used for this analysis consists of a total of 18 982 preselected $\tau^+\tau^-$ pairs, which were culled from the original $Z^0$ decay samples with an efficiency of approximately 92%. The process of preselecting $\tau^+\tau^-$ pairs is performed in two stages, each placing increasingly tighter requirements on the event samples. In the first stage, the dominant background sources are identified and removed. Cosmic ray events are detected through the application of careful timing consistency checks. Electromagnetic calorimeters, located just outside the Z-chambers and in the endcaps (see Figure 3), help

to identify the $e^+e^-$ events, in which nearly all of the initial energy is dumped into the calorimeter. Muon identification is performed by a pair of muon detectors, which make up the outermost layers of both the barrel and endcap regions of the detector. Events resulting in a $\mu^+\mu^-$ pair are flagged if exactly two high-energy muons are identified. Finally, the $q\bar{q}$ events resulting in multihadronic showers are removed by requiring that there be no more than 8 charged tracks in the final state. The second stage of preselection then serves primarily as a check on the operational level of the most important subdetector modules, including the vertex and jet chambers, by placing requirements on the detector status levels of each. Additionally, events in which the $\tau^-$ momentum is too close to the beam axis (i.e., $|\cos\theta| > 0.9$) are dropped because their low transverse momentum makes for poor tracking resolution.

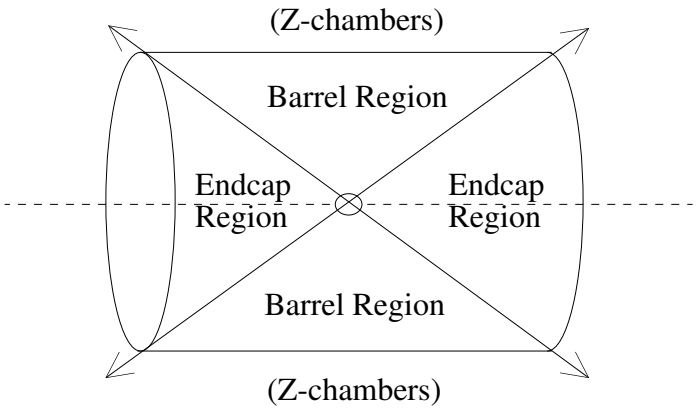


Figure 3: *Locations of the barrel and endcap regions of the detector. The decay products of barrel region events leave the detector via the "sides" of the cylinder, where the Z-chambers are positioned to track their path.*

## 3.2 The Monte Carlo Samples

Two separate Monte Carlo samples were used to complement the two data samples from 1990 and 1991. At the physics level, a collection of pure $\tau^+\tau^-$ decays were produced by the KORALZ [3] Monte Carlo generator. The raw physics output from KORALZ was then fed into the OPAL Collaboration's detailed detector simulator GOPAL [4], which simulates the tracking, interactions, decays, and overall evolution of the $\tau^-$ decay products in the OPAL detector. GOPAL is an extensive and meticulously maintained Monte Carlo simulator, which evolves as the detector evolves; thus, the disparities between the 1990 and 1991 geometries are also manifest in the corresponding versions of GOPAL. The final output produced by GOPAL is identical in format to the real data received from the detector, allowing the same preselection and analysis code to be used on all the data, real and Monte Carlo, 1990 and 1991.

## 3.3 Vertex Finding

The key to identifying the $K_s^0$ in $\tau^-$ decays involves finding the secondary vertex (or neutral V) that is observed when the $K_s^0$ decays inside the detector into $\pi^+\pi^-$ (see Figure 4). Thus, it is essential that an effective algorithm for finding candidate vertices is used to reduce the amount of data in the samples. The algorithm chosen for this analysis is a simple iterative, two-dimensional computer-based search. A pseudo-code outline of the procedure is given below.

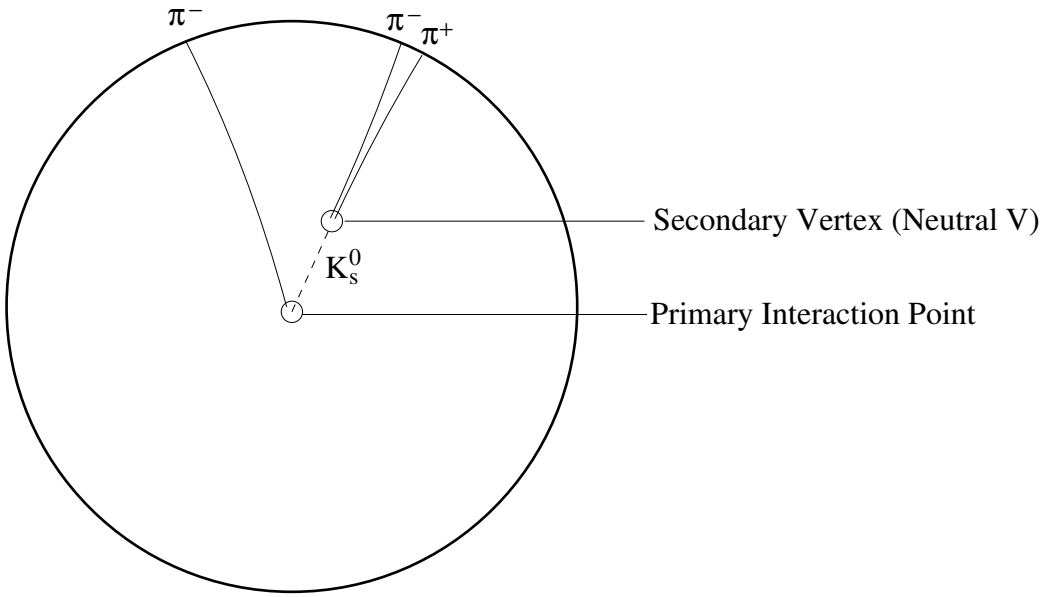


Figure 4: *A typical* $\tau^- \to K_s^0 X^- \nu_\tau$ *event, projected into the r-*$\phi$ *plane. The original* $\tau^-$ *(not shown) decays within the first few millimeters with an average lifetime of 0.3 ps. Note that the* $K_s^0$ *leaves no track and can only be detected indirectly through its decay products.*

```
Begin loop over pairs of oppositely-charged tracks
   Fit circles to the projections of the two tracks
   Determine the points of intersection
   Record only the most plausible intersections (if any)
End loop
```

The procedure begins by finding all possible paired combinations of positive and negative tracks in an event and iterating over them. The only other criterion for this preliminary selection is a loose quality check on the tracks, each of which is required to have registered at least 20 out of a maximum 159 jet chamber hits. Each three-dimensional helical track is then projected into the $r$-$\phi$ plane, and a circle fitted to this projection. By examining only the transverse components of the track, where resolution is far greater, the complications of determining a three-dimensional point of intersection with only rough position measurements in the $z$-direction are greatly reduced.

The vertex reconstruction algorithm next calculates the geometric intersection of the circles from the two oppositely-charged tracks, keeping only those points which might reasonably be found within the detector volume ($r < 150$ cm). Additionally, any intersections found at a radius of less than 1 cm are assumed to originate from the primary interaction point and dropped. A further requirement is that the $\Delta z$ between the two tracks at the calculated point of intersection be less than 20 cm.

For the remaining candidates (if any), a pseudo-$\chi^2$ is then calculated, representing the overall quality and plausibility of the vertex reconstruction. This pseudo-$\chi^2$ is determined by two quantities: the $\Delta z$ from above and the sine of the angle $\delta$ between the reconstructed momentum vector of the neutral particle in the $r$-$\phi$ plane and its flight path vector to the calculated decay vertex (Figure 5). These two quantities are folded in with the expected uncertainties ($\sigma_{\Delta z} = 5.0$ cm and $\sigma_{\sin\delta} = 0.015$) to produce the pseudo-$\chi^2$ distribution. A nominal cut on this quantity, requiring that the pseudo-$\chi^2$ be less than 25, is used to eliminate any exceedingly poor candidates; a more demanding cut, based on the probability distribution extracted from the pseudo-$\chi^2$, is used later in the selection process. In the event that two points of intersection still remain, only the point with the lower pseudo-$\chi^2$ is retained. A final, three-dimensional fit is then performed to determine the $z$ position of the vertex, and the candidate is kept for further scrutiny.

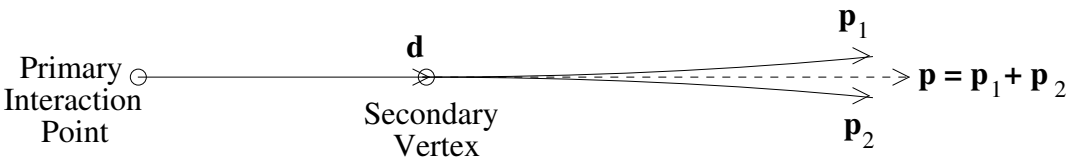


Figure 5: *Ideally the two vectors* **d** *and* **p** *should be parallel. The measured angle between them is the* $\delta$ *used in determining the pseudo-*$\chi^2$*.*

The approach this algorithm uses to locate vertices is clearly a brute-force technique, and there are quite naturally some problems associated with using it. The primary side-effect is the inclusion of false vertices, where two unrelated tracks by sheer chance happen to pass all the cuts. Fortunately, by the application of further, more demanding cuts described below, this artifact can be almost completely eliminated. In addition, by relying on precise geometric intersections to determine vertex candidates, the algorithm runs the risk of missing real vertices altogether, e.g., in the case where two tracks are reconstructed in such a way that they just barely miss each other. The net result is a loss in detection efficiency on the order of 18%, as determined from the Monte Carlo samples.

More serious, however, are the fundamental difficulties associated with the apparatus and track reconstruction. A significant number of decay vertices are lost when the $K^0_s$ decays outside the central detector, where there is no further tracking data, or within the first 1 cm, where they are indistinguishable from any of a number of three-particle $\tau^-$

decays. Monte Carlo estimates of $K_s^0$ decays at LEP energies show that these two effects account for nearly 10% of all lost $K_s^0$ events. Furthermore, in the case of a late-decaying $K_s^0$, there is no guarantee that both decay products will achieve enough jet chamber hits to be properly reconstructed, or even identified as a track at all. Together, all of these geometrical limitations contribute to a net 25% loss in the original signal.

While a more elegant approach to vertex finding might have been able to recoup some of the efficiency losses due to the missing vertices, there are inevitably trade-offs associated with using them. An alternate method that was considered involved finding the points on the fitted circles where the two tracks had parallel tangents. The $r$-$\phi$ coordinates of the vertex position were then taken to be the midpoint of the line connecting these two points. Although this method proved to be more efficient at locating the vertices themselves, it produced unsatisfactory momentum resolution due to the additional fitting step that was required to determine the $r$-$\phi$ momentum at the calculated vertex location. For this analysis, then, the brute-force approach using geometric track intersections was deemed acceptable.

## 3.4 Background Determination

As a first step, the process of selecting vertex candidates serves as a rough cut on the data sample; however, the background remaining still dominates the signal by a factor of roughly 20:1. In order to determine both the nature of these background events as well as the best means of removing them, the Monte Carlo samples were examined and the sources identified. Plot 1 gives a general overview of these various sources.

By far the most dominant background source is the false vertices that are picked up by the vertex reconstruction algorithm. Events in this category consist of a pair of particles, either with different parents or of unlike types, which by chance passed the rather loose cuts in the vertex finding process. Essentially, the algorithm has picked two particles at random; therefore, it is expected that most of these spurious candidates will be removed by tighter cuts, as the signal they represent should be random noise, which is flat in the limit of high statistics.

Photon conversions, $\gamma \to e^+e^-\gamma$ (and to a much lesser extent, $\pi^0 \to e^+e^-$ conversions) also comprise a significant portion of the background events. This is to be expected, as the track signatures for both types of events are identical to that of the $K_s^0 \to \pi^+\pi^-$ decay (a neutral particle decaying into an oppositely-charged pair), and the photon conversions in particular are a common occurrence. Identification of these events is relatively straightforward, as the reconstructed mass of the neutral parent particle should be considerably smaller than the $K_s^0$ mass of 498 MeV/$c^2$.

The interaction of charged mesons with the material in the detector presents an additional source of background events. Typical reactions involve a $\pi^-$ or $K^-$, produced in the original $\tau^-$ decay, interacting with nucleons in the detector material to produce multi-pion final states. For example, the reaction

$$\pi^- p \to n\pi^+\pi^-(n\pi^0)$$

produces a secondary vertex in the detector which is picked up by the vertex finding algorithm. On occasion, such reactions can give a total of four or more charged pions,

each oppositely-charged pair a potential candidate. In all these cases, however, the decay products in the rest frame of the parent particle are no longer produced back-to-back, as in the case of the two-body $K^0_s \rightarrow \pi^+\pi^-$ decay, and this provides a handle that can be used to identify these events. Furthermore, after reconstructing the mass of the parent from only two of the many final state particles, it is unlikely (though possible) that this will fall near the $K^0_s$ mass.

There are also several direct decays of the $\tau^-$ which contribute low-level background noise to the sample of secondary vertices. The two most prominent of these are the decays:

$$\tau^- \rightarrow \pi^+\pi^-\pi^+\pi^0\nu_\tau$$

and

$$\tau^- \rightarrow a_1^-(1260)\nu_\tau \rightarrow \pi^+\pi^-\pi^+\nu_\tau.$$

Although the radii of these decay vertices should theoretically be contained within the first 1 cm, inaccuracies in tracking, reconstruction, and vertex fitting can be responsible for smearing the true vertex location away from the primary interaction point. In this case, as with the multi-pion interactions described above, the lack of a back-to-back decay in the rest frame of the parent as well as the inconsistent reconstructed mass will together help to eliminate nearly all of these events.

Finally, the existence of several $K^0_s$ events that were not produced via the decay of a $K^{*-}(892)$ present a troubling problem. The source of these spurious $K^0_s$ in the Monte Carlo simulations is entirely due to secondary interactions in the detector, perhaps of the form $K^-p \rightarrow K^0_s n$. With the Monte Carlo data, then, it should be possible to trace back one step further and reconstruct the mass of the $K^0_s X^-$ system. By requiring that this mass be sufficiently close to the $K^{*-}(892)$ mass, nearly all of this background would be eliminated. However, it is not known for certain that the $K^{*-}(892)$ is really the one and only source of $K^0_s$ in $\tau^-$ decays, so applying this analysis to the data involves a potentially invalid assumption that could cover up the existence of other means of $K^0_s$ production. Instead, the contribution these events make to the background must be estimated using the Monte Carlo and its effect removed directly.

## 3.5 Selection Criteria

The reduction of background noise serves as the motivation behind the more stringent selection criteria described in this section. In the process of locating secondary decay vertices, a total of 3833 candidates were found, of which perhaps 5% correspond to a true $K^0_s \rightarrow \pi^+\pi^-$ decay. In order to be identified as a true $K^0_s$ decay, then, each candidate is required to satisfy the following criteria.

1. *The transverse momentum, $p_t$, of each track in the oppositely-charged pair must lie between 150 MeV/c and 45.7 GeV/c.* This very loose cut is required to ensure accuracy in the vertex fit. Very low-$p_t$ tracks tend to spiral when projected into the $r$-$\phi$ plane, making it difficult to fit a circle and perform an accurate vertex fit. The upper limit simply represents the maximum possible momentum of a track produced at the LEP center-of-mass energy. Any tracks from a secondary vertex

that are found to have a momentum above this threshold are assumed to have been incorrectly reconstructed.

2. *Each charged track in the pair must either register at least 4 out of a maximum 6 hits in the Z-chambers, or have a z-coordinate measurement in the endcap (Plot 2.)* Because momentum resolution in all three dimensions is very important for an accurate reconstruction of the $K_s^0$ mass, it is essential that a reliable indication of the forward momentum—which is the least accurately measured component—be available. The justification for requiring 4 or more hits in the Z-chambers simply stems from the experimental observation that tracks entering the Z-chambers under normal conditions nearly always register at least 4 hits. If a track misses the Z-chambers, instead exiting via the endcaps, its $z$-momentum can be found by determining at which point the particle left the detector and extrapolating back to the interaction vertex.

3. *The probability, determined from the vertex's pseudo-$\chi^2$, that represents the likelihood of the vertex fit must be greater than 0.05.* In determining the pseudo-$\chi^2$ for the vertex candidates, it was hypothesized that the uncertainty distribution of the two parameters $\Delta z$ and $\sin\delta$ would roughly approximate a true $\chi^2$ distribution. By mapping the distribution actually found to a flat probability between 0 and 1, using the same transformation as for a proper $\chi^2$, the validity of this hypothesis can be more easily determined. When this mapping is actually done, the probability distribution is found to be flat with a sharp tail on the lower end, indicating an inconsistency between the data and the $\chi^2$ hypothesis (Plot 3). By placing a cut at 0.05, the bulk of this tail is eliminated at the expense of relatively few conformant events.

4. *In addition to the two tracks which make up the vertex, at least one additional charged track of good quality must be present in the same hemisphere as the vertex.* This requirement is the result of simple charge conservation. The $\tau^+\tau^-$ pair that results from the decay of the $Z^0$ is produced back-to-back, making it logical to assign a hemispherical volume to each tau, into which its future decay products will be produced. If the $\tau^-$ then decays almost immediately into a $K_s^0$, charge conservation dictates that an additional charged particle must be produced into the same hemisphere. In order to be considered a "good quality" track, this charged particle must have registered at least 40 jet chamber hits with a transverse momentum greater than 150 MeV/c and a distance of closest approach to the primary interaction point of less than 2 cm in the $r$-$\phi$ plane and less than 50 cm along the $z$ direction. Further requirements (e.g., that there be specifically an odd number of these tracks) were not made because the loss in detector efficiency that accompanies events with many tracks can cause either some tracks to be missed or a single track to be interpreted as two separate tracks.

5. *The angle $\theta^*$ between the momentum of the outgoing $\pi^\pm$ and the flight path vector of the $K_s^0$, measured in the $K_s^0$ rest frame, must satisfy $|\cos\theta^*| < 0.9$ (Figure 6).* For a pure collection of two-body $K_s^0$ decays, the distribution of $\cos\theta^*$ should in theory be flat. In practice, however, the distribution shows a definite bias toward the values $\pm 1.0$ (Plot 4), primarily as a result of reconstructing a two-body decay vertex from

the products of a many-body interaction (e.g., the $\pi^- p \rightarrow n\pi^+\pi^-\pi^0$ interaction described above), which is no longer a symmetric decay in the rest frame of the incorrectly reconstructed "parent." The net result is that when these two particles are forced into this rest frame, any asymmetry in their momenta will manifest itself as a bias toward the extreme values of $\cos\theta^*$. By keeping only those events whose $|\cos\theta^*|$ is less than 0.9, most of this bias is removed, leaving behind a roughly flat distribution.

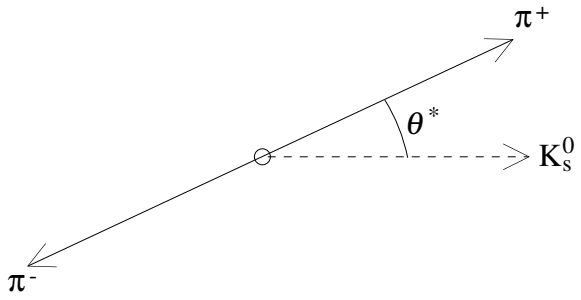


Figure 6: *Definition of the angle $\theta^*$, measured in the rest frame of the* $K^0_s$.

6. *The reconstructed mass of the neutral parent, under the assumption that the two oppositely-charged tracks are an $e^+e^-$ pair, must be greater than 100 MeV/$c^2$.* The sole purpose of this cut is to eliminate any remaining photon conversion vertices from the data sample. Because the lab-frame momenta of the two tracks are known, their vector sum should produce the momentum of their neutral parent. Additionally, if an assumption is made regarding the masses of the two particles, their individual energies can be calculated, along with the total energy of the decay system. These two pieces of information together specify the mass of the neutral parent particle via the basic relativistic mass-energy relationship. Thus, if the masses of the two decay products are assumed to be equal to the electron mass, then most photon conversions will have a reconstructed mass near zero. With a cut at 100 MeV/$c^2$, nearly all of this significant background is eliminated.

7. *The value of the pseudo-$\chi^2$ for the given candidate must be the lowest of all vertex candidates in that event.* This cut serves as a final defense against the contamination of many-body decay vertices. Unwanted interactions in the detector as well as multi-pion $\tau^-$ decays can often lead to several pairs of tracks being picked up as vertex candidates. However, for a decay or interaction that results in more than two final state particles, the reconstructed momentum vector of a given pair of them will tend not to point back to the primary interaction point, a factor which is folded into the pseudo-$\chi^2$ calculation for that vertex candidate. By keeping only the candidate with the lowest pseudo-$\chi^2$ in an event, many of these extra pairs are eliminated. It is then expected that the $K^0_s$ events will typically have the best pseudo-$\chi^2$ of all remaining vertex candidates, a hypothesis which is borne out by the Monte Carlo event sample.

8. *The invariant mass of the decay system, assuming a $\pi^{\pm}$ mass for the two decay products, must lie within 15 MeV/$c^2$ of the* $K_s^0$ *mass.* This final cut serves as the most important discriminant used to select the true $K_s^0$ decays from the remaining background. In order to determine exactly where to place this all-important cut, the invariant mass distribution is plotted and its statistical properties examined. The combined 1990/1991 distribution of the invariant mass is given in Plot 5, after the application of all other cuts. A Gaussian fit to the data places the center of the peak at $497.2 \pm 2.2$ MeV/$c^2$, with a width of $13.3 \pm 2.2$ MeV/$c^2$. Statistically, then, the choice of a 15 MeV/$c^2$ threshold (at $1.125\sigma$, roughly the half-width at half-maximum) will result in a final data sample containing a majority of the true $K_s^0$ decays with very few marginal events. The final cut is made there.

With all the selection cuts in place, the Monte Carlo event sample becomes dominated by signal events, as seen in Plot 6 for the two years being examined. In the data, a net total of 65 candidate $K_s^0$ decays remain, divided between the two years with 18 events from 1990 and 47 events from 1991. For each year, a distribution very similar to Plot 5 was plotted and fitted as before to a Gaussian signal with an exponentially decaying background. From the latter function, the magnitude of the background contamination under the peak was calculated and found to be on the level of 5.6 events in 1990 and 6.2 events in 1991. An additional source of contamination, arising from $K_s^0$ decays which did not originate with a $\tau^-$, was then estimated using the Monte Carlo and found to consist of 0.14 events in 1990 and 1.8 events in 1991. These two values were then subtracted from the total event counts to give a net observed signal of $N_{90}^{\rm obs} = 12 \pm 3.5$ events and $N_{91}^{\rm obs} = 40 \pm 6.3$ events.

## 3.6 Efficiency Determination

Together, the vertex-finding algorithm plus the selection criteria above produce a relatively clean sample of $K_s^0$ events. In order to determine a value for the branching ratio $\tau^- \to K_s^0 X^- \nu_\tau$ however, the efficiency with which this process is able to extract the $K_s^0$ decays becomes important. As a means of determining a value for this efficiency, the selection process was applied to the Monte Carlo sample and the ratio of $K_s^0$ selected to $K_s^0$ physically produced was found. Extracting $K_s^0$ events from the 1990 Monte Carlo revealed an efficiency $\epsilon_{90} = (31.1 \pm 2.5)\%$, while in the 1991 sample it was $\epsilon_{91} = (28.3 \pm 1.6)\%$.

As a check on these values, the Monte Carlo and real data distributions for all the selection variables were plotted and the effects of the cuts on each sample compared. In this process, a significant discrepancy between the 1990 data and the corresponding Monte Carlo was found (see Plot 2). The track quality cut requiring 4 Z-chamber hits or a $z$-coordinate measurement from the endcap eliminated a much larger percentage of data events ($35.7 \pm 4.1\%$) than Monte Carlo events ($20.4 \pm 1.3\%$). Because this cut is expected to affect all types of events equally, such a discrepancy reveals a flaw in the efficiency calculated using the Monte Carlo. To correct for this, it was assumed that this cut affected the detection efficiency independently of all the others, such that $\epsilon_{90}^{\rm tot} = \epsilon_{90}^{\rm cut} \epsilon_{90}^{\rm others}$. If this is held to be true, then simply dividing out the Monte Carlo efficiency and factoring in the real $\epsilon_{90}^{\rm cut}$ as determined from the data will give the correct result. The correction factor actually applied to the 1990 efficiency was $0.808 \pm 0.053$,

giving a corrected efficiency $\epsilon_{90}^{\rm corr} = 25.2 \pm 2.6\%$. As shown in Plot 2(b), this discrepancy does not appear in the 1991 data sample.

# 4 Final Results

Before proceeding with the branching ratio calculation, a plot was made of the $K_s^0$ lifetime for all remaining events (Plot 7). In an effort to estimate the shape of the background, both Monte Carlo background events as well as real background events taken from the side-bands of Plot 5 (events between 35 and 50 MeV/$c^2$ away from the $K_s^0$ mass) were used. Within the statistical limits of the side-band events, the two background shapes agreed very well, which was taken as confirmation that the Monte Carlo distribution was accurate. Subtracting this background and fitting an exponential to the histogram (excluding the first bin, which is missing many events because of the vertex cut at 1 cm), a mean lifetime of $\tau_{K_s^0} = 72^{+20}_{-13}$ ps was found, consistent with the Particle Data Group value of 89 ps.

In order to determine the total number of $K_s^0$ mesons produced in the $\tau^-$ sample examined, correction factors both for the efficiency of detection and for the existence of unobserved $K_s^0$ decays were applied to the number of observed signal events, giving

$$N^{\rm true} = \left( \frac{N_{90}^{\rm obs}}{\epsilon_{90}^{\rm corr}} + \frac{N_{91}^{\rm obs}}{\epsilon_{91}} \right) \frac{\sigma(K_s^0 \rightarrow \text{anything})}{\sigma(K_s^0 \rightarrow \pi^+\pi^-)}.$$

The branching ratio for $K_s^0 \rightarrow \pi^+\pi^-$ is known to be 68.6% to a high degree of accuracy, resulting in a final total of $N^{\rm true} = 275.4 \pm 40.5$ events. Dividing this by the total number of $\tau^\pm$ in the sample results in a branching ratio of

$$B(\tau^- \rightarrow K_s^0 X^- \nu_\tau) = (0.73 \pm 0.11)\%.$$

Comparing this with the current Particle Data Group value of $(0.65 \pm 0.15)\%$ reveals the two values to be consistent to within less than $1\sigma$.

Identification of the $K_s^0$ source was then attempted by reconstructing the mass of its parent, under the assumption that the $K_s^0$ and the first good quality charged track in the same hemisphere were both produced via the decay of this particle. For this part of the analysis, only cadidates with a single additional charged track in the vertex hemisphere were considered. A histogram of the results is given in Plot 8, along with a fit to the data which identifies the parent particle's mass as $890 \pm 20$ MeV/$c^2$. Clearly, the $K^{*-}(892)$ is the primary culprit, with only 1 event having an invariant mass inconsistent with this particle. The Monte Carlo shows an occasional inconsistency as well, despite its inability to produce a $K_s^0$ from a $\tau^-$ decay without the accompanying $K^{*-}(892)$. Thus, it is a reasonable assumption that this anomalous event merely represents background, quite likely due to the contamination of an occasional $K_s^0$ produced in a secondary interaction. Under the assumption, then, that the only source of $\tau^- \rightarrow K_s^0 X^- \nu_\tau$ decays is via a $K^{*-}(892)$ resonance, an estimate of the $\tau^- \rightarrow K^{*-}(892)\nu_\tau$ branching ratio can be made. Since the $K_s^0\pi^-$ final state represents a simple 33% of all $K^{*-}(892)$ decays, the estimated branching ratio is found to be

$$B(\tau^- \to \mathrm{K}^{*-}(892)\nu_\tau) = (2.2 \pm 0.3)\%,$$

which is once again consistent with the $(1.4 \pm 0.9)\%$ reported by the Particle Data Group.

To date, the measurement of a branching ratio for $\tau^- \to \mathrm{K}^0_\mathrm{s}\mathrm{X}^-\nu_\tau$ has been attempted only once before [1]. It is primarily the lack of a statistically significant sample that has prevented a more extensive analysis from being made. Clearly, even this analysis is severely limited by statistical errors; however, with the additional data expected from LEP and OPAL in 1992–1993, this analysis can be repeated to achieve not only a better resolution measurement of the branching ratio but also a more accurate understanding of the $\tau^- \to \mathrm{K}^0_\mathrm{s}\mathrm{X}^-\nu_\tau$ decay process.

# Plot Captions

Plot 1. *The distribution of background events after vertex selection in (a) the 1990 Monte Carlo sample, and (b) the 1991 Monte Carlo sample.*

Plots 2–4. *These plots serve as comparisons between the data and Monte Carlo distributions in the variables used for cuts. In each plot, the data is shown as points with error bars, while the Monte Carlo (normalized to the number of data events) is drawn as a histogram. Each distribution is plotted after all cuts except the final cut on the invariant $\pi^+\pi^-$ mass and the cut relevant to the variable displayed. The location of the proposed cut is given by a dotted line.*

Plot 2. *The number of Z-chamber hits registered by the tracks making up the vertex candidate. Only the hit count for the track with the lowest number of hits is plotted, because the requirement that* both *tracks have 4 or more hits means that the lower of the two ultimately determines the fate of the vertex candidate. The distributions for (a) 1990 and (b) 1991 are separated to show the efficiency discrepancy between data and Monte Carlo under the cut placed at 4 hits. Only events to the right of the cut boundary are kept.*

Plot 3. *The probability distribution for vertex candidates, calculated from their pseudo-$\chi^2$. The significant tail near zero indicates that the events there do not conform to the true $\chi^2$ uncertainty distribution; a cut placed at 0.05 (the dotted line) effectively removes this inconsistent data. The small tail near one also indicates disagreement with the $\chi^2$ hypothesis; however, because these events represent the best vertex candidates, they are not removed at this stage.*

Plot 4. *The $|\cos\theta^*|$ distribution, where $\theta^*$ is defined as in Figure 6. For a true, two-body decay, this distribution should be flat. The sharp tails on the ends arise when the momenta of the two daughter particles are asymmetric in the rest frame of the decaying parent, which is often the case for two particles taken from a many-body decay. The cut requiring $|\cos\theta^*| < 0.9$ removes most of this contamination.*

Plot 5. *The combined 1990/1991 invariant mass distribution of the final vertex candidates. The points with error bars represent the data, whose shape was fitted to a Gaussian distribution with an exponential background. The histogram shown is the background estimate from the Monte Carlo samples, normalized such that the total number of events remaining after all cuts is equal between the two samples; the signal events were then removed from the Monte Carlo. The* $\chi^2$ *of the fit and the fit parameters* $p_1 \ldots p_5$ *are listed in the upper-right. The role of the fit parameters is as follows:*

$$y = p_1 \exp\left[\frac{(x - p_2)^2}{2p_3^2}\right] + \exp(p_4 + p_5 x).$$

Plot 6. *The distribution of background events after all selection criteria have been applied to (a) the 1990 Monte Carlo sample, and (b) the 1991 Monte Carlo sample.*

Plot 7. *Lifetime distribution of the* $\mathrm{K}^0_\mathrm{s}$ *candidates remaining after applying all cuts and removing the estimated background. The fit was made to the data (points with error bars) with an exponential curve of the form* $y = \exp(p_1 + p_2 x)$*, excluding the first bin. The histogram shown represents the Monte Carlo prediction of this distribution.*

Plot 8. *The invariant mass distribution of the* $\mathrm{K}^0_\mathrm{s}\pi^-$ *system for the final* $\mathrm{K}^0_\mathrm{s}$ *candidates, after background subtraction. A Gaussian fit to the data is shown, consistent with a* $\mathrm{K}^{*-}(892)$ *mass of 890 MeV/*$c^2$*.*

# References


[1] R. Tschirhart et al., Phys. Lett. **B205** (1988) 407.

[2] OPAL Collaboration, K. Ahmet et al., Nucl. Instr. and Meth. **A305** (1991) 275.

[3] S. Jadach, B.F.L. Ward, and Z. Was, Comp. Phys. Comm. **66** (1991) 276.

[4] J. Allison et al., CERN-PPE/91–234. Submitted to Nucl. Instr. and Meth., December, 1991.